EDGE ARTICLE

Multifunctional chiral silanol ligands for enantioselective catalysis†

Yun-Pu Chang,[a] Kevin Blanco-Herrero,[a] Turki M. Alturaifi,[b] James C. Fettinger, [ID][a] Peng Liu [ID][b] and Annaliese K. Franz [ID] *[a]

We report transition metal catalysis using novel chiral metal-chelating ligands featuring a silanol coordinating group and peptide-like aminoamide scaffold. The catalytic properties of the silanol ligand are demonstrated through an enantioselective Cu-catalyzed N–H insertion affording unnatural amino acid derivatives in high selectivity. Our investigations into the silanol coordination mode include DFT calculations, ligand structure investigations, and X-ray structure analyses, which support the formation of an H-bond stabilized silanol-chelating copper carbenoid complex. A π–π stacking interaction revealed by DFT calculations is proposed to enable selectivity for aryl diazoacetate substrates, overcoming some of the traditional limitations of using these substrates.

Introduction

Enantioselective catalysis is widely considered as the most efficient method to prepare enantioenriched compounds.[1–3] In metal-catalyzed reactions, chiral ligands are utilized to control reactivity and stereoselectivity. Considerable efforts have been made to design and synthesize classes of ligands[4,5] where heteroatom coordinating sites are key to chiral ligand design principles[6,7] allowing for stereocontrol and tuning of reactivity. Common metal-coordinating groups include phosphines,[8–12] phosphites,[13–15] amines,[8,16] imines,[17,18] and alcohols[16–21] (Fig. 1A).[7] Although silicon has been incorporated in the backbone of a chiral ligand scaffold,[22–27] and the hydridosilane introduced as a coordinating group,[28–33] there are no examples of silanols in metal-coordinating ligands for transition-metal catalyzed enantioselective synthesis.
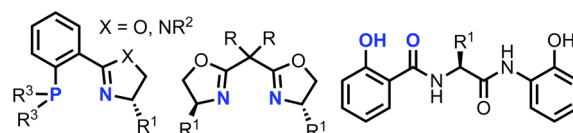
The silanol (Si–OH) group provides an opportunity to design ligands with new coordination modes for enhanced activity and stereoselectivity in asymmetric catalysis. Metal siloxides are more Lewis acidic than metal alkoxides due to back-bonding interactions $(O_{lp} \rightarrow \sigma^*_{Si-C})$[34,35] and the angle-dependent donor capacity of metal siloxides may bring balanced reactivity to catalytic cycles.[36,37] Furthermore, longer Si–O bonds can contribute to improved steric modulation and selectivity. Achiral silanols have been previously utilized as ancillary ligands for a variety of metal-catalyzed transformations[38] such as alkyne metathesis,[37,39,40] Pd-catalyzed cross-coupling[41–44] and *ortho*-metalation.[45–49]

Strohmann has reported chiral zinc(II)-silanoates,[50] including a stereogenic-silicon silanoate,[51] although no catalytic activity was documented. Bolm reported a notable example of a ferrocene-based chiral organosilanol ligand for an asymmetric phenyl-transfer reaction with stoichiometric zinc reagents.[52] In this work, we have developed a novel modular multifunctional chiral ligand scaffold possessing silanol and amide coordination sites (Fig. 1B). This class of ligand overcomes current limitations in substrate scope for the N–H insertion reaction and represents the first example of a silanol in a chelating ligand for transition-metal catalyzed enantioselective synthesis.

Results and discussion

At the start of our investigation, we envisioned incorporating a silanol chelating group into tunable chiral oxazoline (**L1**) and

[a]Department of Chemistry, University of California, Davis, One Shields Avenue, Davis, CA 95616, USA. E-mail: akfranz@ucdavis.edu

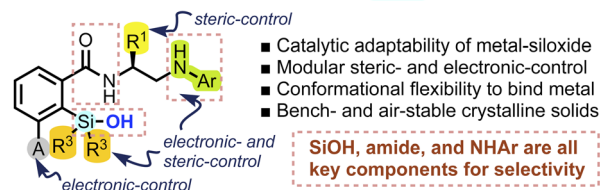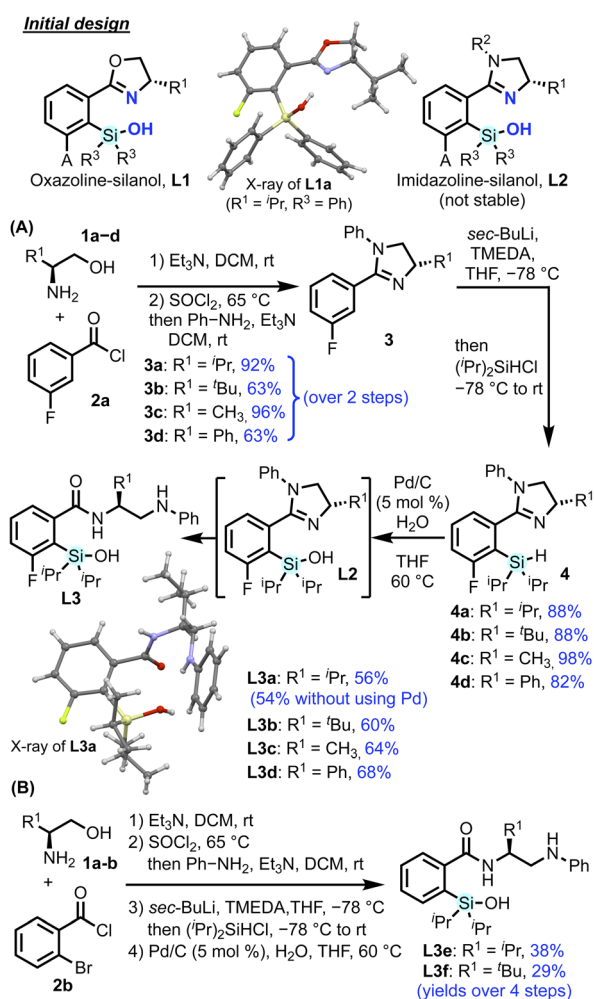[b]Department of Pittsburgh, 219 Parkman Avenue, Pittsburgh, PA 15260, USA

Fig. 1 (A) Common ligands and coordinating groups in asymmetric catalysis. (B) This work: silanol coordinating group in a multifunctional chiral ligand design.

imidazoline (**L2**) scaffolds which serve as common ligands in various enantioselective transformations (Scheme 1).[4,52–55] While **L1** showed poor reactivity and selectivity in several test reactions, attempts to synthesize and evaluate imidazoline-silanol **L2** (ref. 11) led to the discovery of a novel aminoamide ligand (**L3**) formed *via* silanol-facilitated ring-opening of the imidazoline (see ESI†).

Following this discovery, we prepared a collection of aminoamide silanol ligands (**L3**) through an efficient modular synthetic sequence (Scheme 1). The general synthetic procedure utilizes amide formation and cyclization to form imidazoline **3**, followed by *ortho*-lithiation[56] and addition of a chlorosilane to afford silane **4**. Silanols **L3** are obtained upon hydrolysis of silane **4** using catalytic Pd/C with H_2O.[57] We also observed that neighboring group participation of the imidazoline promotes formation of silanol **L3a** without requiring a Pd/C catalyst (see ESI†). This route from inexpensive starting materials is scalable up to 1.5 grams. All of the aminoamide silanol products are air-stable, crystalline white solids.[58] Synthesis *via* silane **4** provides unique access to **L3**; hydrolysis of the corresponding silyl

chloride and attempts at direct silylation of the amide were not successful (see ESI†).

To demonstrate the silanol as a novel coordinating group for transition metal catalysis, an enantioselective copper-catalyzed N–H insertion reaction serves as a model reaction to highlight our preliminary discoveries and overcome the traditionally low selectivity of aryl diazoacetate in this reaction (Fig. 2).[59–69] While initial experiments utilizing oxazoline-silanol **L1** resulted in poor enantioselectivity, the remarkable improvement using silanol **L3a** highlights the importance of the aminoamide backbone. Notably, silanol ligand **L3** enables N–H insertion reactions to be performed without a glovebox or Schlenk line, while still maintaining high enantioselectivity. Following initial success with **L3a**, we optimized the reaction conditions including [Cu] source, solvent, temperature and reaction concentration (see Table S4†). The absence of copper resulted in no reaction, and addition of NaBArF is essential for selectively. While a high background rate is observed without ligand **L3**, no enantioselectivity is observed. No disiloxane formation is observed with **L3** under reaction conditions, and the silanol

Scheme 1 Initial ligand design and synthesis for chiral aminoamide silanol ligands **L3a–d** (A) and **L3e and f** (B).
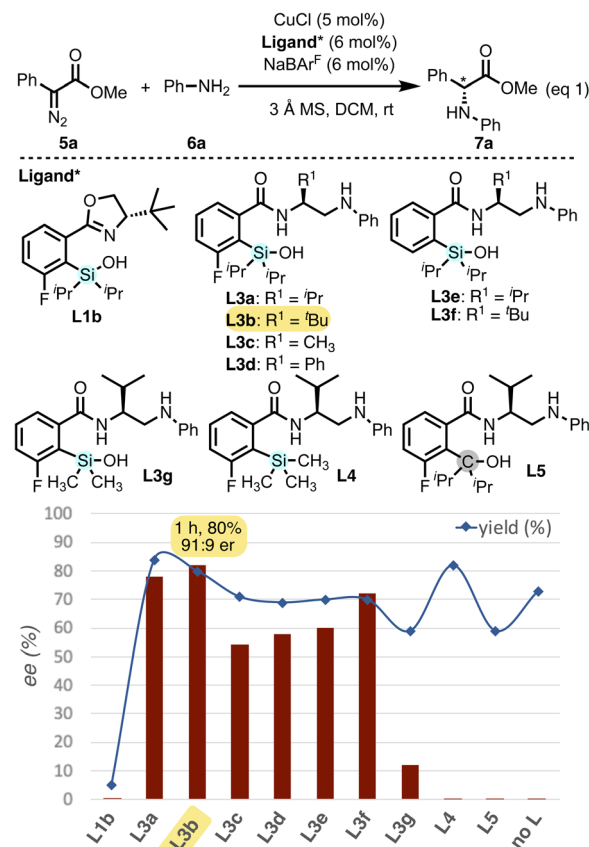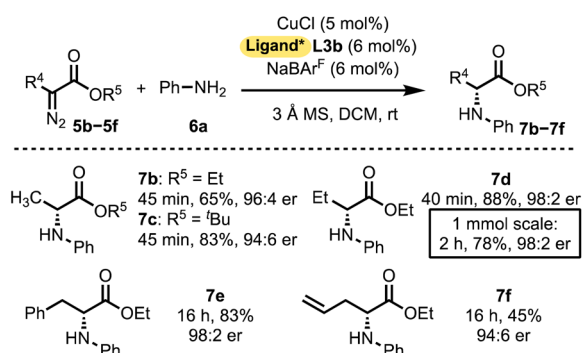

Fig. 2 Ligand optimization for enantioselective N–H insertion of α-phenyl-α-diazoester with aniline (see ESI† for raw data). Standard reaction conditions: **5a** and **6a** (0.2 mmol, 1.0 equiv. each) in DCM (0.05 M) at 23 °C in 1 h; **L3c** 2 h. **L1b** required 16 h for 74% (60 : 40 er, opposite enantiomer); however, 1 h timepoint for **L1b** is graphed for direct comparison. Yield determined using NMR spectroscopy with Ph-TMS as internal standard. Enantiomeric excess (ee%) determined using CSP-HPLC analysis with a Chiralpak OD-H column.

ligand can be reisolated using column chromatography.[70] When the SiOH is replaced with a TMS (**L4**)[71] or COH (**L5**), a complete loss of enantioselectivity is observed, albeit the background rate still proceeds from unchelated copper catalyst (see Table S5† for more control experiments).
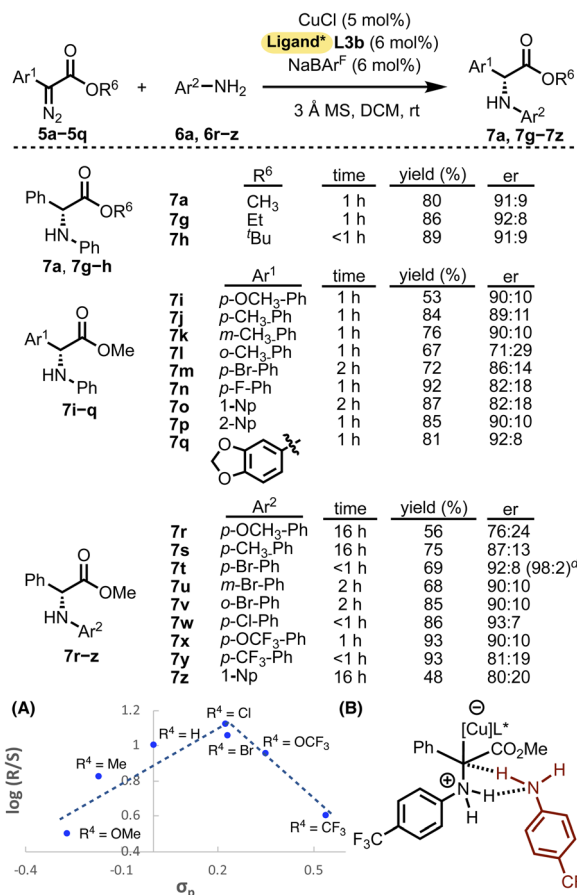
To evaluate the modular ligand components we synthesized a series of silanol ligands (**L3b–L3g**) (Fig. 2). The enantioselectivity of the N–H insertion (**L3a–d**) is influenced by the steric groups (R^1) at the stereogenic center; however, **L3a** and **L3b** exhibit similar performance (89 : 11 and 91 : 9 er, respectively). The fluoro on the core aryl ring was originally incorporated for synthetic purposes, yet a slight reduction in enantioselectivity was observed for **L3e** and **L3f** (80 : 20 and 86 : 14 er, respectively). Ligand **L3g** with a less sterically demanding dimethylsilanol group resulted in a significant decrease in enantioselectivity (89 : 11 *vs.* 56 : 44 er).

Next we evaluated the substrate scope for the enantioselective N–H insertion reaction using silanol ligand **L3b**. The reaction proceeds in high enantioselectivity (94 : 6 to 98 : 2 er) using various alkyl diazoesters **5b–f** with aniline (Scheme 2). And the catalytic performance is unaffected by scaling up to 1.0 mmol scale. The silanol ligand also facilitates high yields with substrates prone to β-H elimination (*i.e.* **7e**), proceeding with reduced side products and enhanced yields, effectively addressing issues reported previously.[68,72] Additionally, the reaction tolerates an olefin (**7f**) under the reaction conditions, exhibiting high selectivity; however, moderate yield was observed due to the inevitable competitive β-H elimination.[73]

The silanol ligand overcomes limitations for previous N–H insertion reactions where α-aryl-α-diazoesters traditionally afford low enantioselectivity; employing silanol **L3b** proceeds with high enantioselectivities for aryl substrates (Scheme 3). The enantioselectivity with phenyldiazoester (91 : 9 er) is not affected by steric modification on the ester (**7a**, **7g** and **7h**). While aryl rings with electron-donating groups afford the highest enantioselectivity, substrates with electron-withdrawing groups also maintain good selectivity. Erosion of enantioselectivity (71 : 29 er) is observed for substitution at the *ortho*-position (**7l**). The electronic profile of the aniline reactant[74] was
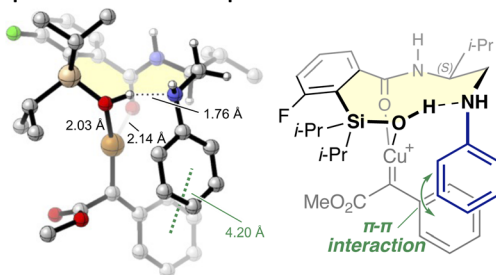

Scheme 3 Scope of the enantioselective N−H insertion of α-aryl-α-diazoesters with anilines providing insight from Hammett plot (A) indicating crossover to proton-shuttle catalysis (B).[a,b,c] [a]Reactions performed under standard reaction conditions. [b]Isolated yields. [c]Determined using CSP-HPLC. The absolute configuration was assigned as (R) based on the HPLC data for **7h**.[76] [d]er determined after recrystallization.
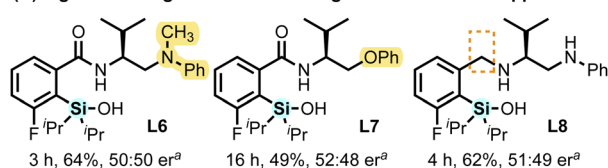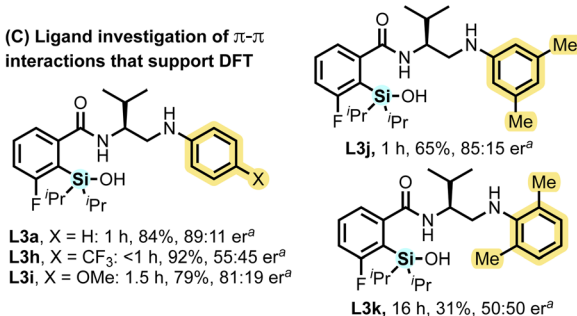
then explored with phenyldiazoacetate (Scheme 3 and **7r–7z**). Interestingly, a crossover point is observed in the Hammett plot (Scheme 3A), indicating a change in mechanism where the strong electron-withdrawing anilines (**7x** and **7y**) start acting as achiral proton-shuttle catalysts, thus leading to a decrease in enantioselectivity (Scheme 3B).[62,68,69,75]

Density functional theory (DFT) calculations reveal the binding mode and conformation of ligand **L3a** in the proposed Cu–carbene complex, supporting the essential role of the silanol as a chelating group in the active complex (Fig. 3A).[62,63,68,69] The isopropyl was utilized in all DFT studies since both **L3a** and **L3b** exhibit comparable performance in the N–H insertion reaction.[77] The analysis demonstrates that the most stable conformation involves both the silanol and amide oxygen atoms coordinating relatively strongly with the copper atom, with bond distances of 2.03 Å and 2.14 Å, respectively. Additionally, intramolecular hydrogen bonding between the silanol and amino group was observed, increasing the Lewis basicity of the silanol oxygen and further stabilizing the silanol–Cu coordination. The ten-membered ring (highlighted in yellow) adopts

Scheme 2 Scope of the enantioselective N−H insertion of α-alkyl-α-diazoesters with aniline.[a,b,c] [a]Performed under standard reaction conditions. [b]Isolated yields. [c]Determined using CSP-HPLC. The absolute configuration was assigned as (R) based on HPLC data for **7d**.[59]

(A) Proposed Cu-carbene complex based on DFT calculations

(B) Ligand investigations of H-bonding interactions that support DFT

L6

3 h, 64%, 50:50 er[a]

L7

16 h, 49%, 52:48 er[a]

L8

4 h, 62%, 51:49 er[a]

(C) Ligand investigation of π–π interactions that support DFT

L3a, X = H: 1 h, 84%, 89:11 er[a]
L3h, X = CF₃: <1 h, 92%, 55:45 er[a]
L3i, X = OMe: 1.5 h, 79%, 81:19 er[a]

L3j, 1 h, 65%, 85:15 er[a]

L3k, 16 h, 31%, 50:50 er[a]

[a]Results from the standard N–H insertion (eq 1)

Fig. 3 (A) The lowest energy conformer of the proposed Cu–carbene intermediate, featuring ligand **L3a** and aryl-diazoesters **5a**, as determined by DFT calculations at the M06/6-311+G(d,p)–SDD(Cu)/SMD(DCM)//B3LYP-D3/6-31G(d)–SDD(Cu) level of theory. Structures of 10 conformers located within 3 kcal mol⁻¹ of the lowest-energy conformer are provided in the ESI;† (B) ligands investigated with different H-bonding capabilities to support DFT; (C) ligands investigated with capabilities for different π–π interactions to support DFT.

Fig. 4 Single-crystal structure of intermediate complex $[(\mathbf{L3a})_2/\mathbf{Na}\cdot(\mathbf{H_2O})_2]^+[\mathbf{BAr^F}]^-$ isolated from slow solvent evaporation over two months. The BAr^F− anion has been omitted for clarity. Selected bond distances (Å), H-bonding interactions, and angles (deg): Si(2)–O(2): 1.634(4), Na(1)–O(2): 2.284(10), Na(1)–O(37): 2.441(8), O(2)–H(2)…N(42), N(18)–H(18)…O(37), N(42)–H(42)…O(13), O(1B)–H(1B1)…N(18), ∠ Si(2)–O(2)–Na(1): 133.7(2).

between the amine and silanol group is critical to promote a favorable conformation that enhances coordination of the silanol to the metal center and imparts enantioselectivity. Without the carbonyl group, **L8** also afforded racemic product, supporting that both the silanol oxygen and the carbonyl oxygen play a key role for coordination in the active complex.

The importance of a π–π interaction is also supported by the distinct influence of the electronic and steric substitution patterns of the *N*-aryl amine in **L3h–k** (Fig. 3C). The analog with a *p*-CF₃ group (**L3h**) shows a loss of enantioselectivity (55 : 45 er) while the *p*-OMe group (**L3i**) retains good enantioselectivity (81 : 19 er). Comparing ligands **L3j** and **L3k**, bearing di-methyl substitution at different positions of the *N*-aryl ring resulted in a complete loss of selectivity and low reactivity for the *ortho*-substituted ligand **L3k**, attributed to steric disruptions of π–π interactions. When conducting the N–H insertion in aromatic solvent, decreased selectivity is observed (78 : 22 er, Table S4†).

An intermediate $[(\mathbf{L3a})2/\mathbf{Na}\cdot(\mathbf{H_2O})_2]^+[\mathbf{BAr^F}]^-$ complex was isolated after slow solvent evaporation and single crystal X-ray analysis supports the formation of H-bond stabilized silanol coordination (Fig. 4). In this intermediate, intramolecular H-bonding interactions are observed between the amino and silanol group, with additional intermolecular H-bonding between amino and amide groups. Although not the active metal complex, the silanol coordination observed in this sodium intermediate is consistent with the DFT calculations, highlighting the role of the silanol as a metal chelating group.[80,81]

Conclusions

Our study details the synthesis and application of new chiral aminoamide silanol ligands for enantioselective catalysis. The silanol group facilitates the formation of a H-bond stabilized

a chair–chair–half-chair conformation[78,79] with no noticeable transannular strain and the isopropyl group placed in the pseudoequatorial position. Moreover, the DFT calculations revealed a π–π interaction between the *N*-phenyl group on the ligand and the phenyl group on the carbene, evidenced by a distance of 4.20 Å between the centroids of the two benzene rings. Traditionally, aryl diazoacetates have yielded low enantioselectivity in the N–H insertion due to aryl stabilization of the free ylide intermediate,[62,68] while alkyl diazoacetates exhibit high selectivity, attributed here to C–H π interactions and lower intermediate stability. Silanol **L3** overcomes this traditional limitation through the proposed π–π interaction, thereby enhancing stability in the metal–ligand complex and catalyst-associated ylide.

To support results of the DFT calculations, silanols **L6–8** were synthesized and evaluated for the enantioselective N–H insertion (eqn (1)) to investigate H-bonding interactions within the metal–ligand complex (Fig. 3B). The *N*-methylated analog (**L6**) affords reduced yield (64%) and no selectivity. Similarly, the phenoxy analog (**L7**) resulted in low enantioselectivity. These observations suggest that the H-bonding interaction
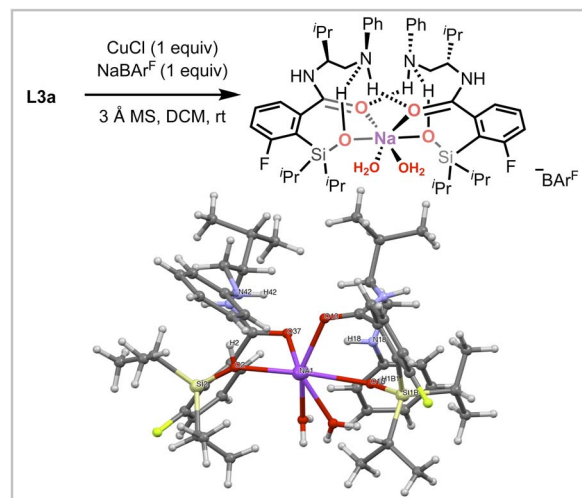
silanol–copper carbenoid active complex, which is supported by DFT calculations, ligand analog studies, and X-ray structural analysis. Our modular ligand design allows access to multiple ligand variants that demonstrate the influence of steric and electronic substituents on activity and selectivity for an N–H insertion reaction. This pioneering use of silanol ligands in transition-metal catalysis provides valuable insights for ligand design and machine learning training sets to allow a more comprehensive understanding of metal–ligand binding interactions and design features for asymmetric catalysis.

Data availability

The data supporting this article have been included as part of the ESI:† experimental procedure, discussion of ligand syntheses characterization data, optimization tables, results of non-linear experiment, copies of spectra, computational details, and Cartesian coordinates of all computed structures are available in the ESI† of this article (PDF). X-ray crystallographic data fare available from the Cambridge Crystallographic Data Centre (CCDC), deposition numbers 2289933 (for **L3a**), 2289935 (for **L3b**), 2289936 (for **3a**), 2289938 (for **S2**), 2289939 (for **L1a**), 2311643 (for $[(\textbf{L3a})_2/\textbf{Na}\cdot(\textbf{H}_2\textbf{O})_2]^+[\textbf{BAr}^{\textbf{F}}]^-$).

Author contributions

Y. P. C. and K. B. H. performed synthetic, spectroscopic and mechanistic studies. P. L. and T. M. A. coordinated and performed DFT calculations and analyses. J. C. F. performed crystallographic analyses. A. K. F. coordinated the experiments and analyses. The manuscript was written through contributions of all authors. All authors have given approval to the final version of the manuscript.

Note after first publication

This article replaces the version published on 13th June 2025, which omitted an NSF award number. The text of the article remains unchanged and the additional NSF award number has been added to the Acknowledgments.

Conflicts of interest

The authors declare no competing financial interest.

Acknowledgements

Notes and references

1 R. Noyori, *Angew. Chem., Int. Ed.*, 2002, **41**, 2008–2022.
2 A. Fanourakis, P. J. Docherty, P. Chuentragool and R. J. Phipps, *ACS Catal.*, 2020, **10**, 10672–10714.
3 D. W. C. MacMillan, *Nature*, 2008, **455**, 304–308.
4 R. Connon, B. Roche, B. V. Rokade and P. J. Guiry, *Chem. Rev.*, 2021, **121**, 6373–6521.
5 T. P. Yoon and E. N. Jacobsen, *Science*, 2003, **299**, 1691–1693.
6 J. F. Hartwig, *Nature*, 2008, **455**, 314–322.
7 J. Margalef, M. Biosca, P. de la Cruz Sánchez, J. Faiges, O. Pàmies and M. Diéguez, *Coord. Chem. Rev.*, 2021, **446**, 214120.
8 W. Zeng, G.-Y. Chen, Y.-G. Zhou and Y.-X. Li, *J. Am. Chem. Soc.*, 2007, **129**, 750–751.
9 A. Pfaltz, I. Drury and J. William, *Chem. Inf.*, 2004, **101**, 5723–5726.
10 G. Helmchen and A. Pfaltz, *Acc. Chem. Res.*, 2000, **33**, 336–345.
11 F. Menges, M. Neuburger and A. Pfaltz, *Org. Lett.*, 2002, **4**, 4713–4716.
12 M. J. Burk, *J. Am. Chem. Soc.*, 1991, **113**, 8518–8519.
13 H. Park, R. Kumareswaran and T. V. RajanBabu, *Tetrahedron*, 2005, **61**, 6352–6367.
14 B. L. Feringa, *Acc. Chem. Res.*, 2000, **33**, 346–353.
15 B. Bartels and G. Helmchen, *Chem. Commun.*, 1999, 741–742.
16 M. C. Schwarzer, A. Fujioka, T. Ishii, H. Ohmiya, S. Mori and M. Sawamura, *Chem. Sci.*, 2018, **9**, 3484–3493.
17 C. A. Krueger, K. W. Kuntz, C. D. Dzierba, W. G. Wirschun, J. D. Gleason, M. L. Snapper and A. H. Hoveyda, *J. Am. Chem. Soc.*, 1999, **121**, 4284–4285.
18 N. S. Josephsohn, K. W. Kuntz, M. L. Snapper and A. H. Hoveyda, *J. Am. Chem. Soc.*, 2001, **123**, 11594–11599.
19 A. Matsuzawa, T. Mashiko, N. Kumagai and M. Shibasaki, *Angew. Chem., Int. Ed.*, 2011, **50**, 7616–7619.
20 K. Narasaka, N. Iwasawa, M. Inoue, T. Yamada, M. Nakashima and J. Sugimori, *J. Am. Chem. Soc.*, 1989, **111**, 5340–5345.
21 E. J. Corey and Y. Matsumura, *Tetrahedron Lett.*, 1991, **32**, 6289–6292.
22 G. T. Notte and J. L. Leighton, *J. Am. Chem. Soc.*, 2008, **130**, 6676–6677.
23 Y. Sakaguchi, Y. Iwade, T. Sekikawa, T. Minami and Y. Hatanaka, *Chem. Commun.*, 2013, **49**, 11173.
24 K. Maruoka, H. Banno and H. Yamamoto, *J. Am. Chem. Soc.*, 1990, **112**, 7791–7793.
25 H. Zhang and D. Zhao, *ACS Catal.*, 2021, **11**, 10748–10753.
26 X. Chang, P. Ma, H. Chen, C. Li and P. Wang, *Angew. Chem., Int. Ed.*, 2020, **59**, 8937–8940.

27 H. F. Sore, W. R. J. D. Galloway and D. R. Spring, *Chem. Soc. Rev.*, 2012, **41**, 1845–1866.

28 B. Yang, J. Gao, X. Tan, Y. Ge and C. He, *Angew. Chem., Int. Ed.*, 2023, e202307812.

29 P. Sangtrirutnugul and T. D. Tilley, *Organometallics*, 2007, **26**, 5557–5568.

30 T. Kitano, T. Komuro, R. Ono and H. Tobita, *Organometallics*, 2017, **36**, 2710–2713.

31 Z. Mo, A. Kostenko, Y.-P. Zhou, S. Yao and M. Driess, *Chem.– Eur. J.*, 2018, **24**, 14608–14612.

32 T. Komuro, D. Mochizuki, H. Hashimoto and H. Tobita, *Dalton Trans.*, 2022, **51**, 9983–9987.

33 T. Komuro, Y. Nakajima, J. Takaya and H. Hashimoto, *Coord. Chem. Rev.*, 2022, **473**, 214837.

34 J. T. Poulton, M. P. Sigalas, K. Folting, W. E. Streib, O. Eisenstein and K. G. Caulton, *Inorg. Chem.*, 1994, **33**, 1476–1485.

35 M. H. Chisholm, F. A. Cotton, M. W. Extine and R. L. Kelly, *J. Am. Chem. Soc.*, 1978, **100**, 3354–3358.

36 A. Fürstner, *Angew. Chem., Int. Ed.*, 2013, **52**, 2794–2819.

37 J. Heppekausen, R. Stade, A. Kondoh, G. Seidel, R. Goddard and A. Fürstner, *Chem.–Eur. J.*, 2012, **18**, 10281–10299.

38 H. Yamagishi, J. Shimokawa and H. Yorimitsu, *ACS Catal.*, 2023, **13**, 7472–7487.

39 A. Fürstner, *J. Am. Chem. Soc.*, 2021, **143**, 15538–15555.

40 J. Hillenbrand, M. Leutzsch, E. Yiannakas, C. P. Gordon, C. Wille, N. Nöthling, C. Copéret and A. Fürstner, *J. Am. Chem. Soc.*, 2020, **142**, 11279–11294.

41 S. E. Denmark and R. C. Smith, *J. Am. Chem. Soc.*, 2010, **132**, 1243–1245.

42 S. E. Denmark, *J. Org. Chem.*, 2009, **74**, 2915–2927.

43 S. E. Denmark and A. Ambrosi, *Org. Process Res. Dev.*, 2015, **19**, 982–994.

44 S. A. Tymonko, R. C. Smith, A. Ambrosi, M. H. Ober, H. Wang and S. E. Denmark, *J. Am. Chem. Soc.*, 2015, **137**, 6200–6218.

45 C. Huang, B. Chattopadhyay and V. Gevorgyan, *J. Am. Chem. Soc.*, 2011, **133**, 12406–12409.

46 C. Huang, N. Ghvatadze, B. Chattopadhyay and V. Gevorgyan, *J. Am. Chem. Soc.*, 2011, **133**, 17630–17633.

47 C. Huang, N. Ghvatadze, B. Godoi and V. Gevorgyan, *Chem.– Eur. J.*, 2012, **18**, 9789–9792.

48 M. Parasram and V. Gevorgyan, *Acc. Chem. Res.*, 2017, **50**, 2038–2053.

49 S. M. Sieburth and L. Fensterbank, *J. Org. Chem.*, 1993, **58**, 6314–6318.

50 C. Golz, P. Steffen and C. Strohmann, *Angew. Chem., Int. Ed.*, 2017, **56**, 8295–8298.

51 F. Langenohl, J. Rösler, S. Zühlke, J. Kirchhoff and C. Strohmann, *Chem.–Eur. J.*, 2023, **29**, e202202935.

52 S. Özçubukçu, F. Schmidt and C. Bolm, *Org. Lett.*, 2005, **7**, 1407–1409.

53 C. C. Bausch and A. Pfaltz, PHOX Ligands, in *Privileged Chiral Ligands and Catalysts*, Wiley-VCH Verlag GmbH & Co. KGaA, 2011.

54 G. C. Hargaden and P. J. Guiry, *Chem. Rev.*, 2009, **109**, 2505–2550.

55 G. Desimoni, G. Faita and K. A. Jørgensen, *Chem. Rev.*, 2006, **106**, 3561–3651.

56 S. O. Wilson, N. T. Tran and A. K. Franz, *Organometallics*, 2012, **31**, 6715–6718.

57 M. Jeon, J. Han and J. Park, *ACS Catal.*, 2012, **2**, 1539–1549.

58 **L3a** was found to be stable to air and atmospheric moisture for >30 months with minimal decomposition and no loss of catalytic activity.

59 B. Liu, S.-F. Zhu, W. Zhang, C. Chen and Q.-L. Zhou, *J. Am. Chem. Soc.*, 2007, **129**, 5834–5835.

60 S.-F. Zhu and Q.-L. Zhou, *Acc. Chem. Res.*, 2012, **45**, 1365–1377.

61 L. G. Furniel, R. Echemendía and A. C. B. Burtoloso, *Chem. Sci.*, 2021, **12**, 7453–7459.

62 D. Gillingham and N. Fei, *Chem. Soc. Rev.*, 2013, **42**, 4918.

63 M.-L. Li, J.-H. Yu, Y.-H. Li, S.-F. Zhu and Q.-L. Zhou, *Science*, 2019, **366**, 990–994.

64 M.-L. Li, J.-B. Pan and Q.-L. Zhou, *Nat. Catal.*, 2022, **5**, 571–577.

65 Z. Liu, C. Calvó-Tusell, A. Z. Zhou, K. Chen, M. Garcia-Borràs and F. H. Arnold, *Nat. Chem.*, 2021, **13**, 1166–1172.

66 W. Yang, M. Pu, X. Lin, M. Chen, Y. Song, X. Liu, Y.-D. Wu and X. Feng, *J. Am. Chem. Soc.*, 2021, **143**, 9648–9656.

67 E. C. Lee and G. C. Fu, *J. Am. Chem. Soc.*, 2007, **129**, 12066–12067.

68 S.-F. Zhu, B. Xu, G.-P. Wang and Q.-L. Zhou, *J. Am. Chem. Soc.*, 2012, **134**, 436–442.

69 Y. Zhu, X. Liu, S. Dong, Y. Zhou, W. Li, L. Lin and X. Feng, *Angew. Chem., Int. Ed.*, 2014, **53**, 1636–1640.

70 The presence of the unaltered silanol ligand **L3** was also confirmed after each N–H insertion through ^{19}F NMR spectroscopy.

71 The diisopropylmethylsilyl is not readily accessible; however, the trimethylsilyl analog (**L4**) serves as a direct comparison with the dimethylsilanol (**L3g**), showing a complete loss of selectivity (50 : 50 er) compared to **L3g**.

72 W.-S. Huang, Z. Xu, K.-F. Yang, L. Chen, Z.-J. Zheng and L.-W. Xu, *RSC Adv.*, 2015, **5**, 46455–46463.

73 P. Guo, Y. Chen, L. Tao, S. Ji, R. Zhang, Z. Zhang, X. Liang, D. Wang, Y. Li and J. Zhao, *ACS Catal.*, 2024, **14**, 4690–4698.

74 When cyclohexyl amine was used under the optimal reaction conditions, no reaction was observed.

75 C. Hansch, A. Leo and R. W. Taft, *Chem. Rev.*, 1991, **91**, 165–195.

76 J.-B. Pan, X.-G. Zhang, Y.-F. Shi, A.-C. Han, Y.-J. Chen, J. Ouyang, M.-L. Li and Q.-L. Zhou, *Angew. Chem., Int. Ed.*, 2023, **62**, e202300691.

77 The distinction between **L3a** and **L3b** is the steric group at the chiral center, which lacks coordination potential in the metal–ligand complex. We chose **L3a** for X-ray studies due to its lower cost and higher availability in the lab. Additionally, **L3a** was used in DFT calculations to ensure consistency with experimental results.

78 V. Dragojlovic, *ChemTexts*, 2015, **1**, 14.

79 K. B. Wiberg, *J. Org. Chem.*, 2003, **68**, 9322–9329.

80 J. C. Slootweg and P. Chen, *Organometallics*, 2006, **25**, 5863–5869.

81 E. Iniesta and A. Vidal-Ferran, *Chem. Commun.*, 2020, **56**, 6364–6367.